ISSN 1330-3651 (Print), ISSN 1848-6339 (Online)
https://doi.org/10.17559/TV-20231224001230
Original scientific paper

Deformation Behaviour and Energy Absorption of 3D Printed Polymeric Gyroid Structures

Yılmaz GÜR

Abstract: This study investigates the deformation behaviour of gyroid lattice structures fabricated via fused deposition modelling 3D printing technology, utilising neat acrylonitrile butadiene styrene and short carbon fibre-reinforced ABS thermoplastics. Initially, a 3D model of the gyroid cellular structure was generated using K3DSurf mathematical software and subsequently 3D printed. The 3D printing layer thickness during the 3D printing process was 150 μm, and the diameter of the filaments was 1.75 mm in diameter. The study employs quasi static uniaxial compression testing to analyse the behaviour of these gyroid lattice structures. The compression tests were performed according to the American Society for Testing and Materials D1621-00 standard. Results indicate distinct deformation behaviours depending on the material used, with short carbon fibre reinforced ABS gyroid cellular structures exhibiting higher strain values and, more energy absorption capabilities compared to neat ABS counterparts. Furthermore, the study highlights the challenges and opportunities associated with fabricating and characterising complex lattice structures, shedding light on their potential applications in engineering disciplines.

Keywords: additive manufacturing; compression test; gyroid short-carbon fibre

1 INTRODUCTION

Additive Manufacturing (AM) technology allows the fabrication of extremely complicated geometrical models that cannot be produced by conventional engineering methods such as cutting, drilling, lathing, and milling [1-3]. The ability to fabricate the structures with intricate details makes AM technology an alternative to traditional engineering manufacturing techniques [4]. Hence, additive manufacturing techniques are especially useful in the biomedical [5, 6], aerospace sectors [7], and automotive industries [8]. In recent years, researchers have paid more attention to lattice structures fabricated by additive manufacturing technologies because of their mechanical energy absorption capabilities and strength-weight ratio performances [4, 9, 10]. They are already used in different engineering disciplines such as customized biomedical implants [11, 12], filters and heat exchangers [13-15], and lightweight structures [16].

Triply Periodic Minimal Surfaces (TPMS) is a specific type of minimal surface characterized by having zero mean curvature, which implies equal concavity and convexity at all points. These surfaces have a hyperbolic form [17]. There are two types of TPMS structures: skeletal-based TPMS cellular structures and sheet-based TPMS cellular structures. For this study, a sheet based TPMS structure, also referred to as a "shellular" structure, is employed [9, 18, 19]. These complex periodic cellular structures offer the potential to design lightweight products that possess excellent energy absorption capabilities.

Several works have been carried out to assess the mechanical properties of sheet based TPMS lattice structures. Zhang et al [10] studied compressive modulus, plateau stress, and energy absorption abilities of P, D, and G types of TPMS sheet structures and reported that TPMS structures greatly outperformed the strut-based lattices. In their study, Maskery et al. [9] conducted research on the energy absorption capacity of gyroid cellular structures. They discovered that heat-treated double gyroid (DG) specimens exhibited an energy absorption capability that was nearly 50% higher compared to body-centred cubic (BCC) structures. The study by Zhang et al. [20] utilizes the response surface methodology (RSM) statistical tool to analyse and optimize the mechanical responses of a BCC lattice structure for passive vibration isolation. Through compression tests, the research identifies the optimal design parameters, demonstrating that RSM is effective in revealing the statistical significance and contribution of input factors to mechanical responses with minimal testing and cost. Moreover, the DG specimens absorbed three times more energy than the BCC structures. Abueidda et al. [21] conducted an analysis of the mechanical performances of 3D-printed structures. They investigated the behaviour of these structures under compressive and tensile loadings through both experimental and computational methods. The researchers found that the mechanical responses of the TPMS cellular structures exhibited reasonable agreement between the experimental and computational results. Gümrük et al. [22] experimentally investigated the mechanical behaviour of micro lattice structures 3D printed by selective laser melting. According to the research, the mechanical behaviour of lattice structures is affected by significant structural defects that arise from the 3D printing process, particularly in shear loading rather than compression. Moreover, the mechanical response of lattice structures is also affected by key parameters such as relative density, cell size, and unit cell topology in all tests. Striemann et al. [23] examined the void content of additively manufactured polymer tensile test specimens using micro-computed tomography. The researchers discovered that the presence of voids had a Notable impact on the material's properties. Specifically, they observed a significant reduction in Young's modulus, tensile strength, and strain at fracture.

Gyroid lattice structures are of interest due to their lightweight nature, and they can be used in many engineering applications. The previous studies on lattice structures fabricated using fused deposition modelling (FDM) have been limited to unreinforced thermoplastic structures [24-26]. A few studies have discussed the use of short carbon fibre reinforced (SCFR) thermoplastic lattice structures. However, printing lattice structures with short carbon fibre reinforced composites can potentially offer advantages such as simultaneous improvement in strength, energy absorption properties, and the stability of crush properties in terms of stable stress-strain behaviour.

Nevertheless, numerical modelling of fibre-reinforced lattice structures under compressive strains is rarely performed, and energy absorption capability calculation through the area under the stress-strain curve and curve fitting is the novelty of the study.

In this study, gyroid lattice structures were printed using 15%-weight short carbon fibre reinforced (SCFR) acrylonitrile butadiene styrene (ABS) and neat acrylonitrile butadiene styrene (ABS) thermoplastic materials by using FDM 3D printing technology. The objective of this study was to conduct experimental research on the deformation behaviour of gyroid lattice structures made of ABS and SCFR-ABS under a quasi-static uniaxial compressive test and to evaluate the energy absorption characteristics of the two different gyroid lattices. To find the energy absorption area under the stress-strain curve, a sixth-degree polynomial was fitted, and the coefficient of determination R^2 was calculated. The SCFR-ABS-made gyroid cellular structure exhibited 1.46 times more energy absorption capability than the ABS-made gyroid.

2 MATERIALS AND METHODS

2.1 Materials and Equipment

TPMS gyroid specimens were manufactured using two types of filaments: light green neat ABS and black Frosch-made short carbon fibre reinforced (SCFR) ABS. The SCFR-ABS filament is a composite material of ABS and contains approximately 15% short carbon fibre by weight. The filaments had a diameter of 1.75 mm. The typical mechanical properties of ABS and short carbon fibre reinforced ABS are given in Tab. 1.

Table 1 Mechanical properties of ABS and SCFR-ABS filaments

Material	Tensile Strength/ MPa	Modulus of Elasticity / GPa	Strain at Break / %
ABS	44	2.07	4.8
SCRF-ABS	59	2.89	3.64

The mechanical properties of ABS and short carbon fibre reinforced ABS materials demonstrates that carbon fibre reinforced ABS generally possesses higher tensile strength and modulus of elasticity compared to ABS. This increase is achieved through the addition of carbon fibre to the material matrix. However, this enhanced durability of SCRF-ABS comes at a cost; SCFR-ABS has a lower strain at break compared to ABS, indicating less flexibility.

Due to the abrasive nature of the short carbon fibre reinforced ABS filament, the original brass nozzle of the 3D printer was replaced with a hardened steel nozzle to maintain a nozzle orifice diameter of 0.4 mm. The gyroid samples were fabricated using a Flash Forge Creator 3D FDM printer, which is equipped with a dual nozzle and a heated build plate covered with kapton tape. Two types of materials were used: short carbon-fibre-reinforced ABS and neat ABS. The layer thickness for both specimens was set to 150 μm. During the fabrication process of the specimens, the build platform temperature was maintained at 100 degrees Celsius.

The gyroid specimens achieved a volume fraction of 0.178, which was determined based on a 1 mm wall thickness.

Table 2 Specifications of the gyroid specimens and printing parameters

	ABS	SCFR-ABS
Cell size / mm	8.33	8.33
Number of lattice unit	6	6
Total number of cells	216	216
Cell wall thickness / mm	1	1
Nozzle temperature	225 ºC	250 ºC
Raft	1 mm	1 mm
Number of outer walls	3	3
Nozzle diameter	0.4	0.4
Nozzle material	Hardened steel	Hardened steel
Printing speed	30 mm/s	30 mm/s
Bed temperature	100 ºC	100 ºC
Layer height	150 μm	150 μm

Additional details regarding the gyroid lattice specimens and 3D printing parameters can be found in Tab. 2.

2.2 Generating of Gyroid Type Triply Periodic Minimal Surfaces (TPMS)

The first triply periodic minimal surface (TPMS), which is the Schwarz P surface, was described by Schwarz in 1890 [27]. Gyroid, in another saying, Schwarz G surface, which is also a member of the TPMS family, is discovered by Alan Schoen while he was studying super-strong, super light structures in 1970. The gyroid is the only example of an intersection-free periodic minimal surface that includes neither straight lines nor mirror reflections, and the axes of rotational symmetry do not lie on the surface. The gyroid is part of the cubic crystal system and has a body centred cubic Bravais lattice. The parameterization of the Gyroid is given by the following equations:

$$x = Re\int \exp\left(i\theta_G\right)F\left(\tau\right)\left(1-\tau^2\right)\mathrm{d}\,\tau \tag{1}$$

$$y = Re\int i\cdot\exp\left(i\theta_G\right)F\left(\tau\right)\left(1+\tau^2\right)\mathrm{d}\,\tau \tag{2}$$

$$z = Re\int 2\cdot\exp\left(i\theta_G\right)\tau F\left(\tau\right)\mathrm{d}\,\tau \tag{3}$$

$$i^2 = 1 \tag{4}$$

$$\tau = \tau_1 + i\tau_2 \tag{5}$$

$$F\left(\tau\right) = \left(1-14\tau^4+\tau^8\right)^{\frac{-1}{2}} \tag{6}$$

Its mathematical equation is highly complex, involving elliptic integrals and it is complicated to solve them [28].

Schnering and Nesper [29] showed that G minimal surfaces can be described to the first order of approximation by the nodal equation which is given in the following Eq. (7). This equation gives an approximation to the gyroid surface looks like the actual gyroid because of that the following approximation Eq. (7) is used to design the six units of gyroid cubic compression test samples [30].

$$\cos x\cdot\sin y+\cos y\cdot\sin z+\cos z\cdot\sin x = 0 \tag{7}$$

To generate the model of the Gyroid, the utilization of mathematical modelling software is necessary. This software performs calculations to determine the x, y, and z coordinate values of the vertex points occurring on the surface. There are various options available in the market for mathematical software, including both commercially licensed and license-free alternatives [31]. These software options offer a range of features and capabilities for conducting mathematical calculations and generating models. For generating the 6-unit cubic gyroid, Eq. (7) is taken into consideration. The mathematical software used for this purpose is K3DSurf v0.6.2. K3DSurf specializes in manipulating multi-dimensional mathematical models and providing visualizations of these models. It offers support for both parametric equations and iso-surfaces [32]. In order to work with K3DSurf, the considered equation should have a right-hand side that evaluates to zero, as per the software's requirement. Eq. (7), which is considered for generating the gyroid, is evaluated with the following boundary Eq. (8) to get the 6-unit gyroid cellular structure.

$$x(-10, 10), y(-10, 10), z(-10, 10) \tag{8}$$

The Eq. (7) is solved with the boundary conditions specified in Eq. (8), employing a grid resolution of 50 × 50 × 50 within the K3DSurf mathematical software. As a result, a six-unit cell gyroid cellular structure was generated and then triangulated. The number of vertices generated during the triangulation process was 38421. The gyroid cellular structure generated based on these vertex points can be seen in Fig. 1.

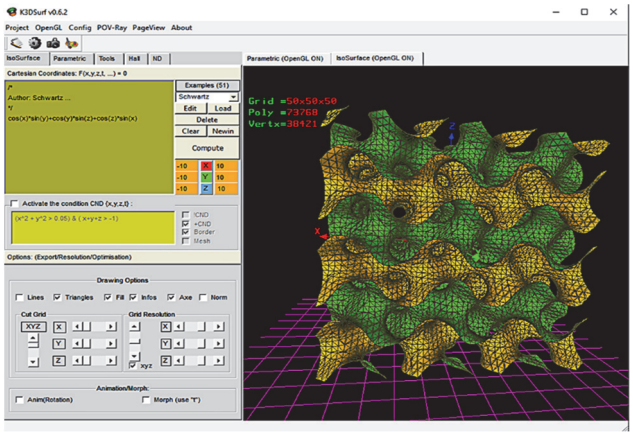

Figure 1 Generating of the gyroid in K3DSurf

The gyroid model generated initially lacks wall thickness, which poses a challenge for its fabrication through 3D printing. To address this issue, the wall thickness of the model is increased to 1 mm using nTopology® advanced additive manufacturing software [33].

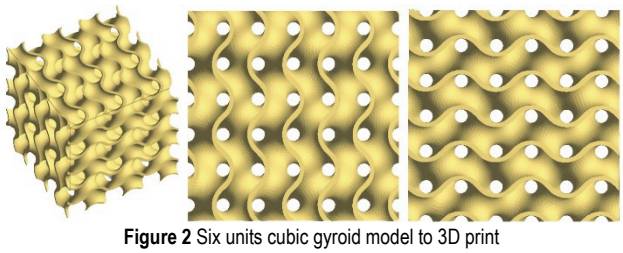

Figure 2 Six units cubic gyroid model to 3D print

By modifying the model with thicker walls, it becomes feasible to 3D print the specimens successfully. Fig. 2 shows the gyroid model after the wall thickness has been increased.

2.3 Specimen Preparation

The Gyroid model is sliced into layers using MakerBot® MakerWare™ v2.4.1.24 software [34]. This slicing software performs several essential functions, including generating travel movements for the printing head, calculating the printing time and filament usage in weight, and creating support structures to ensure stable connections. Fig. 3a. and Fig. 3b. display images of the manufactured specimens, showcasing both the 6 units of ABS gyroid and SCFR-ABS gyroid.

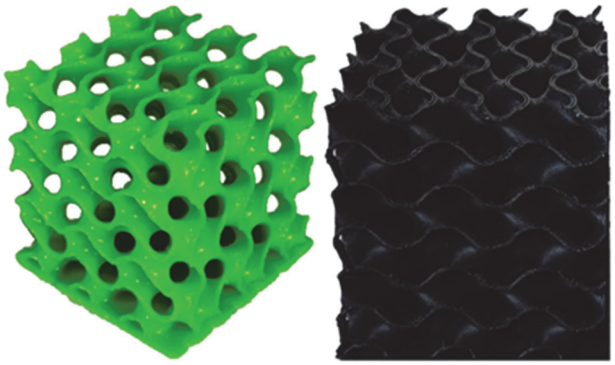

(a) ABS gyroid specimen (b) SCFR-ABS gyroid specimen

Figure 3 3D FDM printed compression test Gyroid specimens

The gyroid cellular lattice specimens used in the testing were cubic in shape with dimensions of 50 × 50 × 50 mm.

2.4 Quasi-static Uniaxial Compression Test

A quasi-static uniaxial compression test of the polymer-based gyroid cellular structures was performed according to the American Society for Testing and Materials (ASTM) D1621-00 standard [35], in which a self-aligning loading heads with a spherical sliding bearing ensured that the load was distributed uniformly during the compressive test. Uniaxial compression experiments were conducted at room temperature around 20 ºC using a Zwick/Roell universal testing machine. A makroXtens BT2-EXMACRO.H11 type extensometer is used as a strain measurement device to measure the displacement of the specimen under compressive load. TestXpert II from Zwick Roell GmbH was used as a testing software. A testControl II control electronics is used for compressive tests, which has a 24-bit resolution with a 400 kHz sampling rate for measured value accuracy and a 2 kHz measured-value logging rate for reproducibility. Four samples of the gyroid cellular structure made of ABS were fabricated, and they were subjected to compression tests for repeatability purposes. The same applies to the samples made of SCFR-ABS (see Fig. 4).

Top-loading compressive testing is performed by applying a downward force to all gyroid cellular structures. A constant compression speed of 0.016 mm/s was used during the compressive testing. The reaction force and

displacement of the compression platens were recorded during the tests. Conversely, the SCFR-ABS gyroid cellular structure exhibits shape deformation starting from the compression surface and progressing toward the bottom.

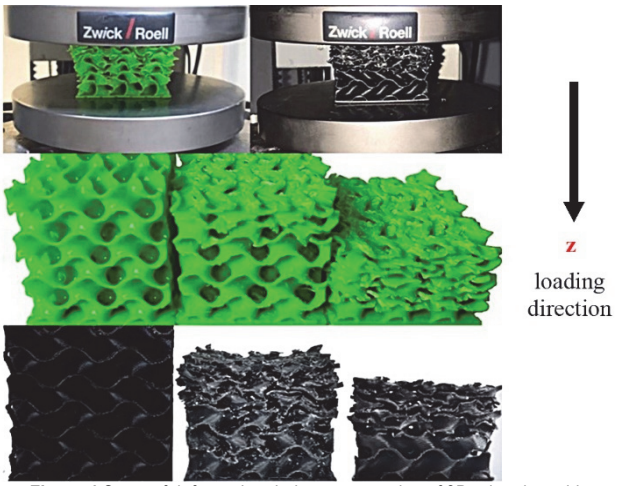

Figure 4 Steps of deformation during compression of 3D printed gyroids

Notably, the final shape changes are observed in the cells located at the bottom under compression. This sequential crushing of cells occurs in planes perpendicular to the loading direction (z), indicating a progressive collapse of the structure.

3 RESULTS AND DISCUSSION

Firstly, each gyroid cellular specimen made of ABS and SCFR-ABS was compressed until 23% of the specimen's height was achieved. (see Fig. 5).

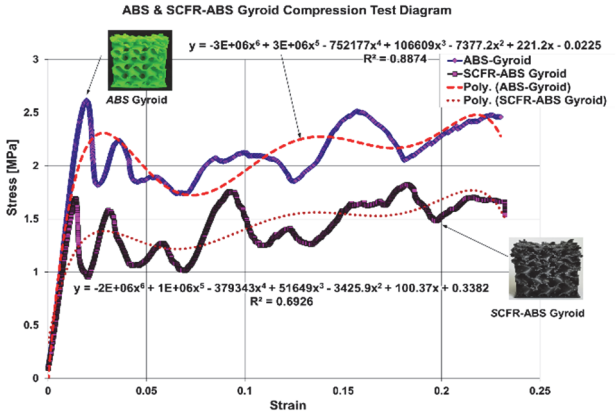

Figure 5 Compressive behaviour up to 23% of the specimen height

The area under the stress-strain curves was calculated using sixth-degree polynomial curves fitted via Microsoft Excel for both specimens. The R-square (R^2) value was calculated as 0.8874. The energy absorption value of the gyroid cellular structure made of ABS material was calculated using the sixth-degree polynomial function as given in Eq. (9).

$$y = -3000000 \cdot x^6 + 300000 \cdot x^5 - 752177 \cdot x^4 + \\ +106609 \cdot x^3 - 7377.2 \cdot x^2 + 221.2 \cdot x - 0.0225 \quad (9)$$

On the other hand, the area under the short carbon fibre reinforced ABS gyroid curve is calculated by using the following sixth-degree polynomial given in Eq. (10). R^2 value for the SCFR-ABS was calculated as 0.6926.

$$y = -2000000 \cdot x^6 + 1000000 \cdot x^5 - 379343 \cdot x^4 + \\ +51649 \cdot x^3 - 3425.9 \cdot x^2 + 100.37 \cdot x + 0.3382 \quad (10)$$

The surface areas based on Eq. (9) and Eq. (10) for the first test samples made of ABS and SCFR-ABS were calculated, and the energy stored per unit volume was 0.955 MJ/m^3 for the ABS sample and 0.655 MJ/m^3 for the SCFR-ABS sample. Energy stored for the ABS sample was 119.375 J and 81.875 J for the SCRF-ABS.

The second compression test was carried out until 48% deformation was achieved for the ABS and SCFR-ABS gyroid cellular structures. The stress-strain curve for compression and deformation of the ABS gyroid was depicted in Fig. 6. The energy absorption value of the ABS gyroid cellular structure was calculated using the sixth-degree polynomial equation given in Eq. (11) using Microsoft Excel. The R2 value was calculated at 0.8065.

$$y = -665481 \cdot x^6 + 679901 \cdot x^5 - 265283 \cdot x^4 + \\ +49130 \cdot x^3 - 4338.1 \cdot x^2 + 160.44 \cdot x + 0.2674 \quad (11)$$

On the other hand, the area under the short carbon fibre reinforced ABS gyroid curve was calculated by using the following sixth-degree polynomial function as given in Eq. (12).

$$y = -36374 \cdot x^6 + 56912 \cdot x^5 - 34258 \cdot x^4 + \\ +9905.5 \cdot x^3 - 1392.4 \cdot x^2 + 83.578 \cdot x + 0.0992 \quad (12)$$

The surface areas based on Eq. (11) and Eq. (12) for the second test samples made of ABS and SCFR-ABS were calculated. The calculated area equals the energy stored per unit volume, and it was 1.34 MJ/m^3 for the ABS sample and 1.48 MJ/m^3 for the SCFR-ABS. Energy stored for the ABS sample is 167.5 J and 185 J for SCRF-ABS. R^2 values for ABS and SCFR-ABS gyroid cellular structures compressed up to 48% of the specimens' height are 0.8065 and 0.7516, respectively. The R^2 values clearly show the relationship between the cumulative energy absorption behaviour and the strain.

Stress and energy absorption curves vs. strain for the compression of ABS and SCFR-ABS gyroid samples, compressed up to 23% and 48% of the specimens' heights, are depicted in Fig. 5 and Fig. 6 respectively.

The stress-strain curves of ABS and SCFR-ABS gyroid specimens shows a drop in the strength of the structure right after the peak strength is reached. This may be result of sudden fracture and collapse of the compressed layer. This causes the lost and recovery of strength consecutively.

The structure becomes stronger after each layer is compressed and densified. As seen in Fig. 5, the initial maximum stress of 2.61 MPa was observed at around 0.01956 strain in the ABS structure. ABS gyroid structure

recovers up to 93% of the initial maximum stress at around 0.16 strain, which is 2.51 MPa.

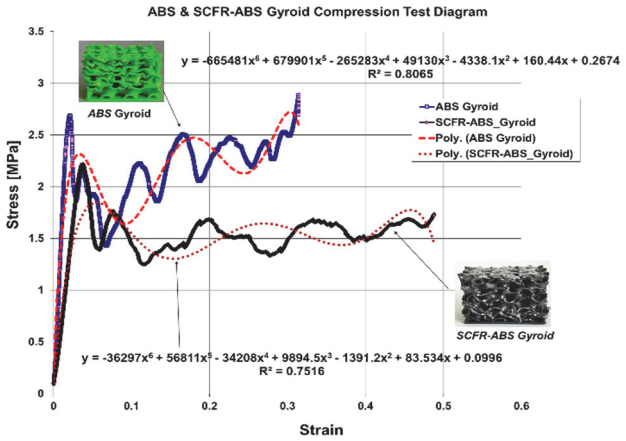

Figure 6 Compressive behaviour up to 48% of the specimen height

The initial maximum compressive stress for the SCFR-ABS cellular structure was 2.2 MPa at 0.014 strain, and just after the deep dropdown, it recovered up to 1.58 MPa at around 0.030 strain. Furthermore, it exceeded the initial maximum stress at around 0.092 strain at 1.76 MPa.

When the ABS gyroid cellular structure was compressed to 48% of its height, the initial maximum stress occurred at 2.69 MPa at approximately 0.021 strain (see Fig. 6). The compression session was stopped by the testing machine at 0.31 strain because of a sudden drop in load. When the compression was stopped, the ABS gyroid structure exceeded the initial maximum stress, which was 2.898 MPa. On the other hand, the initial maximum compressive stress for the SCFR-ABS cellular structure was 2.16 MPa at 0.022 strain. When the SCFR-ABS compressed to 48.81% strain, the stress value was 1.73 MPa (see Fig. 6).

High strength values are obtained for the ABS gyroid cellular structures during the compression tests. However, their strain values were lower than the SCFR-ABS ones. The lower stress values of the SCFR-ABS compared to the ABS could be due to the higher 3D printing temperature of the SCFR-ABS filaments. The higher 3D printing temperatures and the addition of short carbon fibres make the SCFR-ABS specimens brittle.

The complex geometry of the gyroid cellular structure makes it difficult to identify the crack initiation area. But this is most likely due to an internal pore defect of the surface. It is also exceedingly difficult to determine the path followed by the cracks coming from inside the gyroid cellular structure. It is impossible to visually detect the initiation of the crack because the samples are fractured into many small fragments. The direction in which the crack propagates through the walls of the gyroid cells has also been reported in the literature that it may bifurcate perpendicular to its direction, and the crack propagating through the structure probably follows a circuitous path [9].

At the end of the second compression test carried out up to 48% of the specimens' height, the gyroid cellular structure made of ABS polymer exhibited a lower strain value compared to the SCFR-ABS gyroid cellular structure. As seen in Fig. 6, both gyroid structures exhibit a significant decline in stress following the first compressive strength maximum. The first layer collapse at about 0.018 strain for the ABS gyroid and 0.014 strain for SCFR-ABS, where these falls begin. Because the individual cell walls come into contact with one another after a layer collapses, both gyroid cellular structures showed multiple stress maxima and minima. Strain-hardening causes the stress to increase at higher strains. The densification of the broken layers strengthens both gyroid structures. The gyroid structures regain some of the maximum initial crushing strength while losing their dimensions, and this behaviour emphasizes the distinct response of gyroid cellular structures under compressive loading.

4 CONCLUSIONS

The research aims to evaluate the manufacturability of ABS and SCFR-ABS gyroid lattice structures with FDM 3D printing technology, as well as their compressive behaviours when subjected to unidirectional compressive load and energy absorption capabilities.

During the compression test of the gyroid cellular structures, a non-linear relation was observed between stress-strain rather than linear.

Sixth-degree polynomial equations were evaluated to calculate the areas under the stress-strain curves, and the results showed that the SCFR-ABS polymer-made gyroid cellular structure absorbed 1.46 times more energy than the ABS-made gyroid cellular structure. This difference in energy absorption can be the reason for the distinct crushing mode type exhibited by the gyroid cellular structures.

Future research could focus on investigating the number and size of the gyroid cellular structure, wall thicknesses, and 3D printing parameters such as layer thickness, printing speed, and printing temperature. It may involve combining short carbon fibres with other reinforcing agents or functional additives to create hybrid composites that optimize energy absorption and enhance specific properties like impact resistance, toughness, crashworthiness, and energy dissipation. Additionally, integrating sensors within SCFR polymer structures to monitor stress, strain, and damage could provide data to optimize energy absorption capabilities and predict failure. Enhancing computational simulation tools and conducting detailed failure analysis to identify weak points will help in better predicting the behaviour of short SCFR polymers under dynamic loading. By focusing on these areas, future research aims to create more efficient, resilient, and versatile 3D short carbon fibre reinforced polymers that excel in energy absorption and meet the demands of various high-performance applications.

5 REFERENCES

[1] Segerman, H. (2012). 3D Printing for mathematical visualization. *The Mathematical Intelligencer, 34*, 56-62. https://doi.org/10.1007/s00283-012-9319-7

[2] Rosen, D. W. (2007). Computer-aided design for additive manufacturing of cellular structures. *Computer Aided Design and Applications, 4*(5), 585-594. https://doi.org/10.1080/16864360.2007.10738493

[3] Thompson, M. K., Moroni, G., Vaneker, T., Fadel, G., Campbell, R. I., Gibson, I., Bernard, A., Schulz, J., Graf, P.,

Ahuja, B., & Martina, F. (2016). Design for additive manufacturing: trends, opportunities, considerations, and constraints. *CIRP Annals-Manufacturing Technology, 65*(2), 737-760. https://doi.org/10.1016/j.cirp.2016.05.004

[4] Plocher, J. & Panesar, A. (2020). Effect of density and unit cell size grading on the stiffness and energy absorption of short fiber-reinforced functionally graded lattice structures. *Additive Manufacturing, 33*, 101171. https://doi.org/10.1016/j.addma.2020.101171

[5] Afshar, M., Anaraki, A. P., Montazerian, H., & Kadkhodapour, J. (2016). Additive manufacturing and mechanical characterization of graded porosity scaffolds designed based on triply periodic minimal surface architectures. *Journal of the Mechanical Behaviour of Biomedical Materials, 62*, 481-494. https://doi.org/ 10.1016/j.jmbbm.2016.05.027

[6] Yan, C., Hao, L., Hussein, A., & Young, P. (2015). Ti-6Al-4V Triply periodic minimal surface structures for bone implants fabricated via selective laser melting. *Journal of the Mechanical Behaviour of Biomedical Materials, 51*, 61-73. https://doi.org/10.1016/j.jmbbm.2015.06.024

[7] Zhu, L., Li, N., & Childs, P. R. N. (2018). Light weighting in aerospace component and system design. *Propulsion and Power Research, 7*(2), 103-119. https://doi.org/10.1016/j.jppr.2018.04.001

[8] Beamler, Business Cases: 3D Printing in the Automotive Industry, Business, (2018). https://www.beamler.com/3d-printing-in-the-automotive-industry/

[9] Maskery, I., Aboulkhair, N. T., Aremu, A. O., Tuck, C. J., & Ashcroft, I. A. (2017). Compressive failure modes and energy absorption in additively manufactured double gyroid lattices. *Additive Manufacturing, 16*, 24-29. https://doi.org/10.1016/j.addma.2017.04.003

[10] Han, L. & Che, S. (2018). An overview of materials with triply periodic minimal surfaces and related geometry: "from biological structures to self-assembled systems". *Advanced Materials, 30*(17), 1705708. https://doi.org/ 10.1002/adma.201705708

[11] Heinl, P., Müller, L., Körner, C., Singer, R. F., & Müller, F. A. (2008). Cellular Ti-6Al-4V structures with interconnected macro porosity for bone implants fabricated by selective electron beam melting. *Acta Biomaterialia, 4*(5), 1536-1544. https://doi.org/10.1016/j. actbio.2008.03.013

[12] Pattanayak, D. K., Fukuda, A., Matsushita, T., Takemoto, M., Fujibayashi, S., Sasaki, K., Nishida, N., Nakamura, T., & Kokubo, T. (2011). Bioactive Ti Metal analogous to human cancellous bone: fabrication by selective laser melting and chemical treatments. *Acta Biomaterialia, 7*(3), 1398-1406. https://doi.org/10.1016/j.actbio.2010.09.034

[13] Jain, P. & Pradeep, P. (2005). Potential of silver nanoparticle-coated polyurethane foam as an antibacterial water filter. *Biotechnology and Bioengineering, 90*(1), 59-63. https://doi.org/10.1002/bit. 20368

[14] Boomsma, K., Poulikakos, D., & Zwick, Z. (2003). Metal foams as compact high-performance heat exchangers. *Mechanics of Materials, 35*(12), 1161-1176. https://doi.org/10.1016/j.mechmat.2003.02.001

[15] Lu, T. J., Stone, H. A., & Ashby, M. F. (1998). Heat transfer in open-cell metal foams. *Acta Materialia, 46*(10), 3619-3635. https://doi.org/10.1016/S1359-6454(98)00031-7

[16] Simone, A. E. & Gibson, L. J. (1998). Effects of solid distribution on the stiffness and strength of metallic foams. *Acta Materialia, 46*(6), 2139-2150. https://doi.org/ 10.1016/S1359-6454(97)00421-7

[17] The Epinet Project. (2023). http://epinet.anu.edu.au/mathematics/minimal_surfaces

[18] Han, S. C., Lee, J. W., & Kang, K. (2015). A new type of low-density material: shellular. *Advanced Materials, 27*(37), 5506-5511. https://doi.org/10.1002/adma. 201501546

[19] Al-Ketan, O., Rowshan, R., & Abu Al-Rub, R. K. (2018). Topology-mechanical property relationship of 3D printed strut, skeletal, and sheet based periodic metallic cellular materials. *Additive Manufacturing, 19*, 167-183. https://doi.org/10.1016/j.addma.2017.12.006

[20] Zhang, L., Feih, S., Daynes, S., Chang, S., Wang, M. Y., Wei, J., & Lu, W. F. (2018). Energy absorption characteristics of metallic triply periodic minimal surface sheet structures under compressive loading. *Additive Manufacturing, 23*, 505-515. https://doi.org/10.1016/j. addma.2018.08.007

[21] Abueidda, D. W, Bakir, M., Abu Al-Rub, R. K., Bergström, J. S., Sobh, N. A., & Jasiuk, I. (2017). Mechanical properties of 3D printed polymeric cellular materials with triply periodic minimal surface architectures. *Materials & Design, 122*, 255-267. https:// doi.org/10.1016/j.matdes.2017.03.018

[22] Gümrük, R., Mines, R. A. W, & Karadeniz, S. (2013). Static mechanical behaviours of stainless-steel micro-lattice structures under different loading conditions. *Materials Science and Engineering: A, 586*, 392-406. https://doi. org/10.1016/j.msea.2013.07.070

[23] Striemann, P., Huelsbusch, D., Mrzljak, S., Niedermeier, N., & Walther, F. (2020). Systematic approach for the characterization of additive manufactured and injection molded short carbon fiber-reinforced polymers under tensile loading. *Materials Testing, 62*(6), 561-567. https:// doi.org/10.3139/120.111517

[24] Maharjan, G. K., Khan, S. Z., Riza, S. H., & Masood, S. H. (2018). Compressive behaviour of 3D printed polymeric gyroid cellular lattice structure. *IOP Conference Series: Materials Science and Engineering, 455*, 012047.

[25] Maconachie, T., Tino, R., Lozanovski, B., Watson, M., Jones, A., Pandelidi, C., Alghamdi, A., Almalki, A., Downing, D., Brandt, M., & Leary, M. (2020). The compressive behaviour of ABS gyroid lattice structures manufactured by fused deposition modelling. *The International Journal of Advanced Manufacturing Technology, 107*, 4449-4467. https://doi.org/10.1007/s00170-020-05239-4

[26] Yánez, A., Herrera, A., Martel, O., Monopoli, D., & Afonso, H. (2016). Schwarz, H.A. (1890). Compressive behaviour of gyroid lattice structures for human cancellous bone implant applications. *Materials Science and Engineering C, 68*, 445-448. https://doi.org/10.1016/j.msec.2016.06.016

[27] Schwarz, H. A. (1890). *Gesammelte Mathematische Abhandlungen*, Springer Berlin, Heidelberg. https://doi.org/10.1007/978-3-642-50665-9

[28] Schoen, A. H. (1970). Infinite periodic minimal surfaces without self-intersections. NASA Technical Note TN D-5541.

[29] Schnering, V. H. G. & Nesper, R. (1991). Nodal surfaces of Fourier series: Fundamental invariants of structured matter. Zeitschrift Für Physik B. *Condensed Matter*, *83*(3), 407-412. https://doi.org/10.1007/BF01313411

[30] Weyhaupt, A. (2023). *Meet the gyroid*. https://plus. maths.org/content/meet-gyroid

[31] Machado, J.A.T., Özdemir, N., & Baleanu, D. (2020). *Mathematical Modelling and Optimization of Engineering Problems, Springer, 30*, 187-196. https://doi.org/10.1007/978-3-030-37062-6

[32] Taha, A. (2023). K3DSurf Software Package. http://k3dsurf.sourceforge.net/

[33] nTopology Software. (2021). https://ntopology.com/

[34] MakerBot® MakerWare™ v2.4.1.24. (2013). 3-D Printing Software. https://www.maker bot.com/3d-printers/apps/makerbot-print/download/

[35] American Society for Testing and Materials. (2016). *Standard Test Method for Compressive Properties of Rigid Cellular Plastics* (ASTM D1621-00

Contact information:

Yılmaz GÜR, Assoc. Prof. PhD
(Corresponding author)
International University of Sarajevo,
Faculty of Engineering and Natural Sciences,
Department of Mechanical Engineering,
Hrasnička cesta 15,
71210 Ilidža, Sarajevo,
Bosnia and Herzegovina
E-mail: ygur@ius.edu.ba